Small Signal Model for Very-Large-Scale Multi-Active-Bridge Differential Power Processing (MAB-DPP) Architecture

Ping Wang, Yenan Chen, Youssef Elasser, Minjie Chen
Power Electronics Research Lab, Princeton University

Background & Motivation

➢ Large-Scale Modular DC Energy Systems

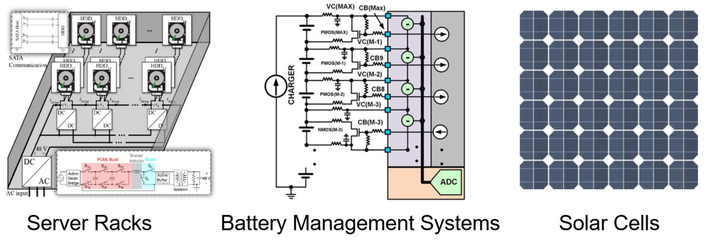

Server Racks | Battery Management Systems | Solar Cells

Fig. 1: Energy systems with numerous modular power converters.

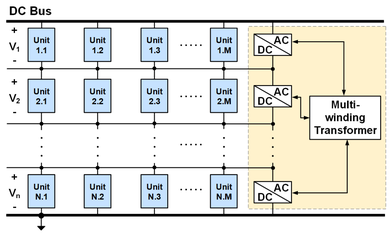

Fig. 2: An example ac-coupled differential power processing (DPP) architecture.

- Differential power processing (DPP) architecture can minimize the power conversion stress and improve the system performance.
- Ac-coupled DPP with a single multi-winding transformer can reduce the component count and improve the power conversion efficiency.

DPP Architecture Comparison

➢ Dc-Coupled v.s. Ac-Coupled DPP Architecture

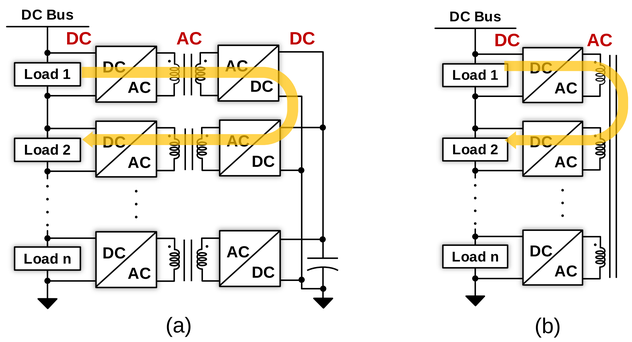

Fig. 3: (a) Dc-coupled DPP architecture; (b) Ac-coupled DPP architecture.

Table II: Advantages of the Ac-Coupled DPP Architecture.

Number of Devices	Dc-Coupled	Ac-Coupled	Benefits
Dc-ac cells	2N	N	50% switches reduction
Transformers	N	1	1/N magnetic volume
Dc-ac-dc stages	2	1	Less conversion stages

- **Advantages:**
  - Higher power density
  - Higher conversion efficiency
  - Lower cost
- **Challenges:**
  - Power flow are closely coupled.
  - Accurate modeling and scalable control strategy is needed for very large scale DPP system.

Systematic Small Signal Modeling Approach

➢ Large-Scale Multi-Active-Bridge Differential Power Processing (MAB-DPP) Architecture

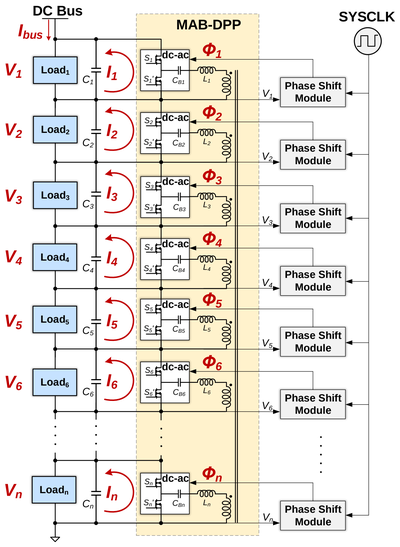

Fig. 4: Large-scale MAB-DPP with distributed phase-shift control.

- **Step 1**. Modeling Large Signal Current:

$$I_i = \frac{P_i}{V_i} = \sum_{j\neq i} \frac{V_j}{2\pi f L_{ij}} \phi_{ij} \left(\frac{|\phi_{ij}|}{\pi} - 1\right) \Rightarrow \frac{\partial I_i}{\partial V_j}, \frac{\partial I_i}{\partial \phi_j}$$

- **Step 2**. Modeling Small Signal Current:

$$\begin{bmatrix} \hat{I}_1 \\ \hat{I}_2 \\ \vdots \\ \hat{I}_n \end{bmatrix} = \begin{bmatrix} 0 & G_{v12} & \cdots & G_{v1n} \\ G_{v21} & 0 & \cdots & G_{v2n} \\ \vdots & \vdots & \ddots & \vdots \\ G_{vn1} & G_{vn2} & \cdots & 0 \end{bmatrix} \begin{bmatrix} dV_1 \\ dV_2 \\ \vdots \\ dV_n \end{bmatrix} + \begin{bmatrix} G_{\phi 11} & G_{\phi 12} & \cdots & G_{\phi 1n} \\ G_{\phi 21} & G_{\phi 22} & \cdots & G_{\phi 2n} \\ \vdots & \vdots & \ddots & \vdots \\ G_{\phi n1} & G_{\phi n2} & \cdots & G_{\phi nn} \end{bmatrix} \begin{bmatrix} \hat{\phi}_1 \\ \hat{\phi}_2 \\ \vdots \\ \hat{\phi}_n \end{bmatrix}$$

$\Downarrow G_v$ $\Downarrow G_\phi$

$$G_{vij} = \frac{\phi_{ij}}{2\pi f L_{ij}} \left(\frac{|\phi_{ij}|}{\pi} - 1\right) \quad G_{\phi ij} = \begin{cases} \frac{V_j}{2\pi f L_{ij}} \left(1 - \frac{2|\phi_{ij}|}{\pi}\right), j \neq i \\ \sum_{j\neq i} \frac{V_j}{2\pi f L_{ij}} \left(\frac{2|\phi_{ij}|}{\pi} - 1\right), j = i \end{cases}$$

- G_{vii} is zero in ideal MAB.

- **Step 3**. Considering the load structure:

$$\begin{bmatrix} \hat{V}_1 \\ \hat{V}_2 \\ \vdots \\ \hat{V}_n \end{bmatrix} = \begin{bmatrix} -Z_1 \| \sum_{k\neq 1} Z_k & \frac{Z_1 Z_2}{\sum_{k=1}^n Z_k} & \cdots & \frac{Z_1 Z_n}{\sum_{k=1}^n Z_k} \\ \frac{Z_2 Z_1}{\sum_{k=1}^n Z_k} & -Z_2 \| \sum_{k\neq 2} Z_k & \cdots & \frac{Z_2 Z_n}{\sum_{k=1}^n Z_k} \\ \vdots & \vdots & \ddots & \vdots \\ \frac{Z_n Z_1}{\sum_{k=1}^n Z_k} & \frac{Z_n Z_2}{\sum_{k=1}^n Z_k} & \cdots & -Z_n \| \sum_{k\neq n} Z_k \end{bmatrix} \times \begin{bmatrix} \hat{I}_1 \\ \hat{I}_2 \\ \vdots \\ \hat{I}_n \end{bmatrix} \Rightarrow G_z$$

- **Step 4**. Obtaining System Transfer Function:

$$\begin{cases} \hat{I} = G_\phi \times \hat{\Phi} + G_v \times \hat{V} \\ \hat{V} = G_z \times \hat{I} \end{cases} \Rightarrow \hat{V} = (I - G_z G_v)^{-1} G_z G_\phi \times \hat{\Phi}$$

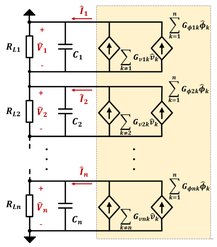

Fig. 5: Small signal model for MAB-DPP without considering losses.

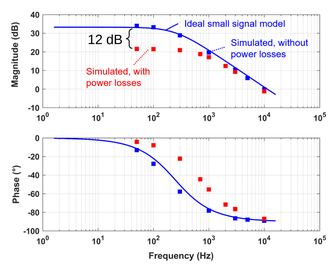

Fig. 6: Simulation verification of a 10-port MAB-DPP converter.

- Derived transfer function matches very well with the simulated bode plot (without considering power losses).
- Power losses reduce the dc gain of the magnitude response and shift the phase response to higher frequency.

➢ Improved Small Signal Model considering Power Losses

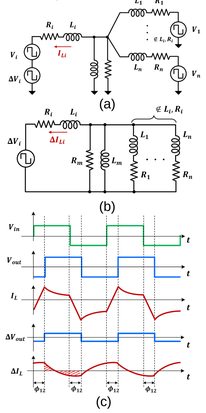

Fig. 7: Operation waveforms of MAB considering losses.

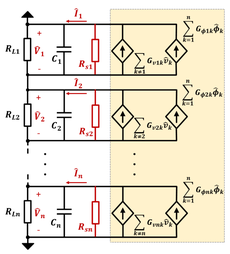

Fig. 8: Improved small signal model.

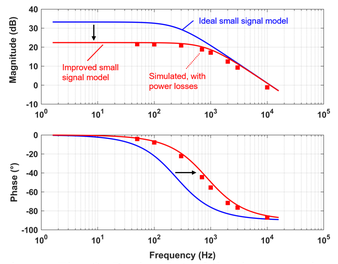

Fig. 9: Bode plot of the improved small signal model.

- Power losses can be modeled as an output resistance R_{si} at each port.
- Output resistance R_{si} is determined by the $\frac{\partial V_i}{\partial I_i}$ at each port.
- Based on the improved small signal model, the calculated bode plot matches well with the simulation results considering power losses.

Large-Scale MAB-DPP Simulation & Control

- Schematic of a 100-Port MAB-DPP Converter.

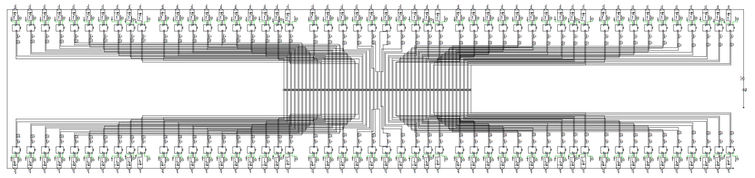

Fig. 10: SPICE simulation platform for a 100-port MAB-DPP system.

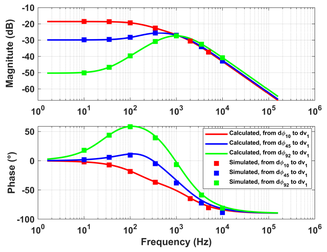

Fig. 11: The calculated and simulated bode plots of three phase to voltage transfer functions.

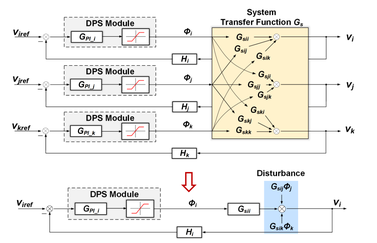

Fig. 12: A modular control strategy with distributed phase-shift (DPS) module.

HDD Storage Server with MAB-DPP

- A 10-Port MAB-DPP Prototype

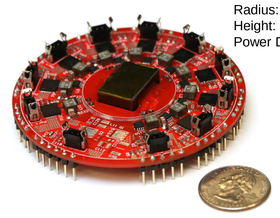

Radius: 3.7 cm
Height: 1.2 cm
Power Density: >100w/in^3

Fig. 13: A 300W 10-port MAB-DPP prototype (with a U.S. quarter).

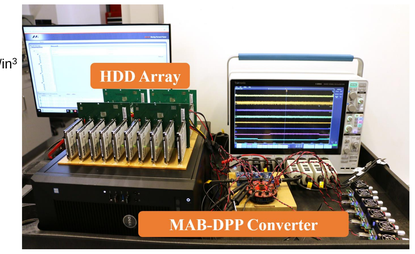

Fig. 14: Testbench of a HDD server with the 10-port MAB-DPP converter.

- Experimental Measurement

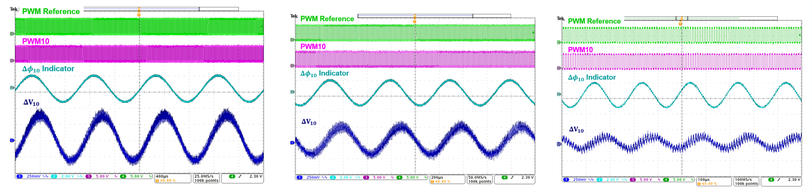

(a) f = 1kHz (b) f = 2kHz (c) f = 5kHz

Fig. 15: Measured voltage perturbation at port 10 ($\hat{v}_{10}$) with a phase perturbation ($\hat{\phi}_{10}$).

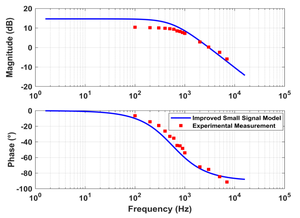

Fig.16: Calculated and measured transfer function from $\hat{\phi}_{10}$ to $\hat{v}_{10}$.

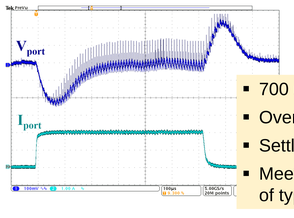

- 700 uF output capacitance
- Overshoot : < 230 mV
- Settling time: < 200 us
- Meet hotswap requirement of typical HDDs (5% VDD)

Fig. 17: Transient response of a port voltage to a 2 A load step change.